A Brain Tumor Segmentation Method Based on CLIP and 3D U-Net with Cross-Modal Semantic Guidance and Multi-Level Feature Fusion *

Ming-Da Zhang

School of Software Yunnan University Kunming, Yunnan Province 650500, China yao110002@gmail.com

ABSTRACT

Precise segmentation of brain tumors from magnetic resonance imaging (MRI) is essential for neurooncology diagnosis and treatment planning. Despite advances in deep learning methods, automatic
segmentation remains challenging due to tumor morphological heterogeneity and complex threedimensional spatial relationships. Current techniques primarily rely on visual features extracted
from MRI sequences while underutilizing semantic knowledge embedded in medical reports. This
research presents a multi-level fusion architecture that integrates pixel-level, feature-level, and
semantic-level information, facilitating comprehensive processing from low-level data to high-level
concepts. The semantic-level fusion pathway combines the semantic understanding capabilities of
Contrastive Language-Image Pre-training (CLIP) models with the spatial feature extraction advantages
of 3D U-Net through three mechanisms: 3D-2D semantic bridging, cross-modal semantic guidance,
and semantic-based attention mechanisms. Experimental validation on the BraTS 2020 dataset
demonstrates that the proposed model achieves an overall Dice coefficient of 0.8567, representing a
4.8% improvement compared to traditional 3D U-Net, with a 7.3% Dice coefficient increase in the
clinically important enhancing tumor (ET) region.

Keywords Brain tumor segmentation \cdot Semantic guidance \cdot Vision-language models \cdot Multi-modal fusion \cdot Deep learning

1 Introduction

Brain tumor segmentation from magnetic resonance imaging (MRI) constitutes a foundational element in neurooncology diagnosis and treatment planning. Gliomas present significant challenges due to their infiltrative growth patterns, morphological heterogeneity, and multiple tumor subregions with varying prognostic significance. Contemporary imaging protocols typically acquire multiple MRI sequences, including T1-weighted, contrast-enhanced T1-weighted (T1ce), T2-weighted, and fluid-attenuated inversion recovery (FLAIR), each providing complementary tissue characteristics. Recent years have witnessed developments in deep learning approaches for brain tumor segmentation, particularly through three-dimensional Convolutional Neural Networks (CNNs) [1], with U-Net and its 3D variants establishing encoder-decoder architectures with skip connections as the predominant framework [2]. Fully automated deep learning networks have shown potential in this domain [3].

Current methods present three main limitations: First, they often utilize single-level feature processing, lacking integrated multi-level information mechanisms [4]; second, they focus predominantly on image data, with limited incorporation of semantic knowledge embedded in medical reports; third, they inadequately model how radiologists integrate multi-level visual information with conceptual understanding during diagnosis. Recent developments in

^{*&}lt;u>Citation</u>: Zhang, M.-D. A Brain Tumor Segmentation Method Based on CLIP and 3D U-Net with Cross-Modal Semantic Guidance and Multi-Level Feature Fusion. arXiv preprint arXiv:XXXXXXXXX (2025).

vision-language models, particularly Contrastive Language-Image Pre-training (CLIP), have demonstrated capabilities in connecting visual and language modalities [5]. Modern attention mechanisms [6] offer potential for enhancing these approaches, though applying these models to 3D volumetric segmentation presents challenges including the dimensional difference between 2D vision-language models and 3D medical volumes, domain shift between natural and medical imagery [7], and requirements for region-level understanding rather than image-level classification.

In this research, we propose a three-layer fusion-based medical vision-language framework applying CLIP to 3D brain tumor segmentation with the following contributions:

- 1. A three-layer fusion architecture incorporating pixel-level, feature-level, and semantic-level information integration, establishing a processing chain from low-level data to high-level concepts [8].
- 2. A semantic-level fusion mechanism that integrates vision-language models with three-dimensional medical data through 3D-2D semantic bridging, cross-modal semantic guidance, and semantic attention mechanisms [9].

2 Related Work

2.1 Brain Tumor Segmentation

Brain tumor segmentation techniques have evolved from traditional image processing to deep learning approaches. The BraTS challenge established standardized evaluation protocols for three clinically important regions: whole tumor (WT), tumor core (TC), and enhancing tumor (ET) [10], providing a benchmark for multimodal CNN networks and segmentation approaches [11]. Current methodologies encompass architectural variations like nnU-Net [12], feature extraction enhancements such as TransBTS [13], and multi-task learning frameworks [14], with comprehensive evaluations identifying effective machine learning algorithms for this task [15].

The three-layer fusion architecture addresses existing limitations by systematically integrating information across multiple levels. This framework implements modality-specific preprocessing at the pixel level, utilizes attentionenhanced U-Net for spatial feature extraction [16], and incorporates CLIP's semantic understanding capabilities at the semantic level, enabling the segmentation process to leverage professional knowledge embedded in medical text descriptions.

2.2 Medical Imaging CLIP Model Optimization

CLIP models demonstrate cross-modal understanding capabilities through contrastive learning from image-text pairs. Applying CLIP to medical imaging presents three principal challenges: dimensional mismatch between 2D models and 3D volumes, domain shift between natural and medical imagery [7], and the requirement for pixel-level precision rather than image-level classification [18]. Medical-specific vision-language pre-training remains predominantly limited to image-level tasks, with limited application to volumetric data processing [19].

To address these limitations, we design a medical CLIP adapter with a 3D-2D semantic bridging mechanism that extracts representative slices from anatomical planes, enhances key features before processing through the CLIP visual encoder, and forms unified 3D understanding through multi-view feature integration [20]. We further implement domain adaptation layers that optimize CLIP's processing capabilities for medical imagery through parameter adjustment and feature transformation.

2.3 Cross-Modal Semantic Guidance and Attention Enhancement

Cross-modal fusion research in medical image analysis has predominantly focused on integrating complementary information across imaging sequences, with limited consideration for incorporating domain knowledge from text modalities. Current fusion strategies employ static processing approaches without semantic-based dynamic adjustment mechanisms [23], with limited incorporation of region-specific descriptions in medical reports and incomplete modeling of radiologists' knowledge-guided visual attention processes [24].

Our approach implements cross-modal semantic guidance through a text-based gating mechanism that modulates visual feature weights according to medical descriptions, adjusting network focus toward clinically significant regions [25]. We develop semantic attention enhancement modules for tumor subregions, generating spatial attention maps through the fusion of decoder features and semantic representations to modulate final segmentation predictions.

3 Methods

3.1 Overall Architecture

We propose a three-layer fusion architecture integrating pixel-level, feature-level, and semantic-level information, as shown in Figure 1. The architecture incorporates a cross-modal semantic guidance mechanism, through which the system utilizes professional knowledge from medical text descriptions to guide the segmentation process by integrating CLIP model's semantic understanding capabilities [17]. This approach addresses dimensional differences between 2D vision-language models and 3D medical data, reflecting the clinical cognitive process of radiologists combining visual observation with conceptual understanding.

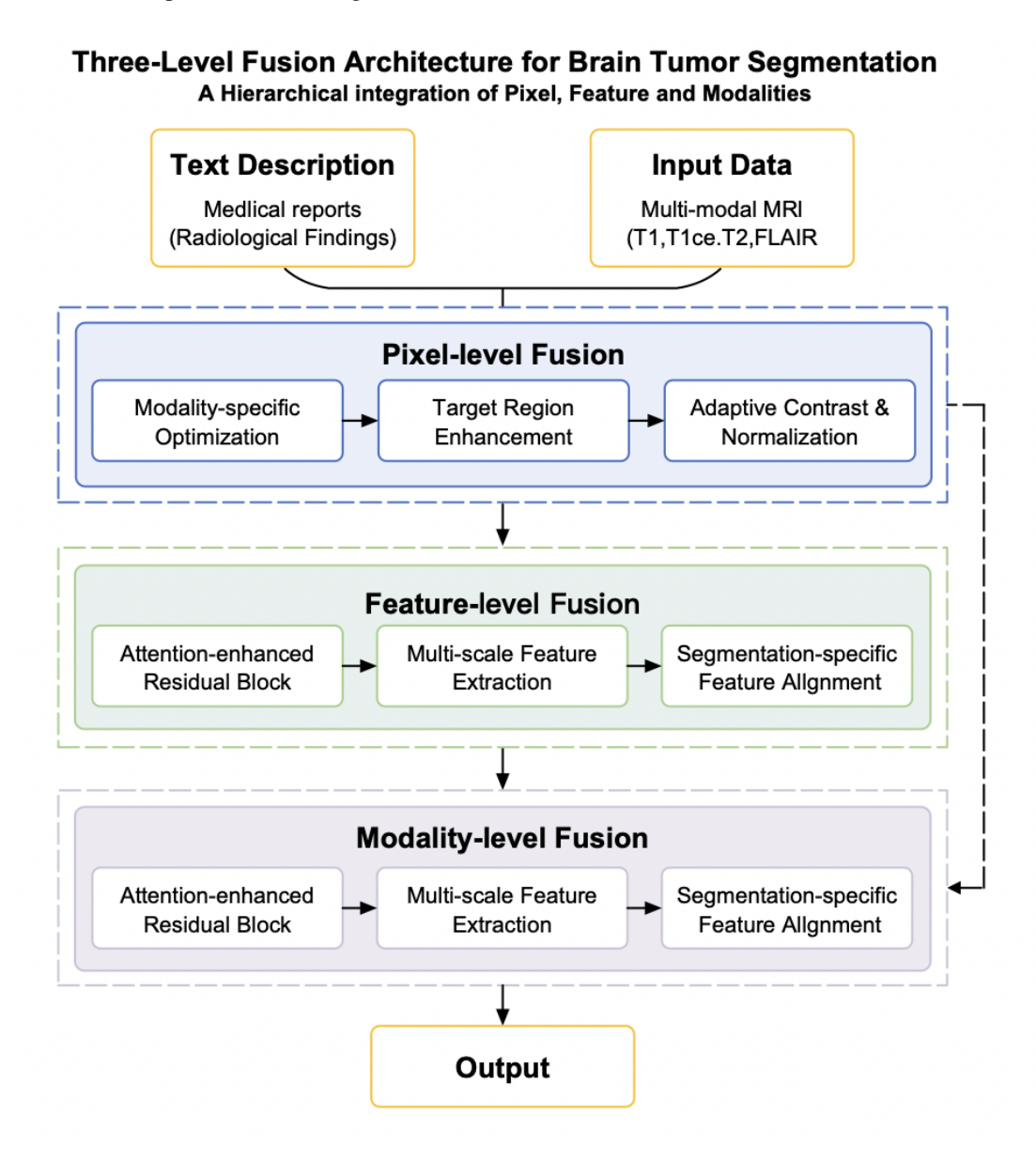


Figure 1: Three-layer fusion architecture diagram

3.2 Pixel-Level Fusion

Pixel-level fusion operates at the raw data representation level, addressing preprocessing and optimization of multi-modal MRI data through modality-specific optimization processing and target region enhancement.

For modality-specific optimization, we apply improved z-score normalization for T1 and T1ce modalities and min-max normalization for T2 and FLAIR modalities. We apply outlier clipping and adaptive contrast adjustment to all modalities, with particular application of non-linear transformations to T1ce sequences to highlight enhancing tumor regions. For target region enhancement, we implement mechanisms for enhancing tumor (ET) and tumor core (TC) regions, applying specific contrast enhancements (approximately 25% contrast magnification for ET regions and 20% for TC regions) [21].

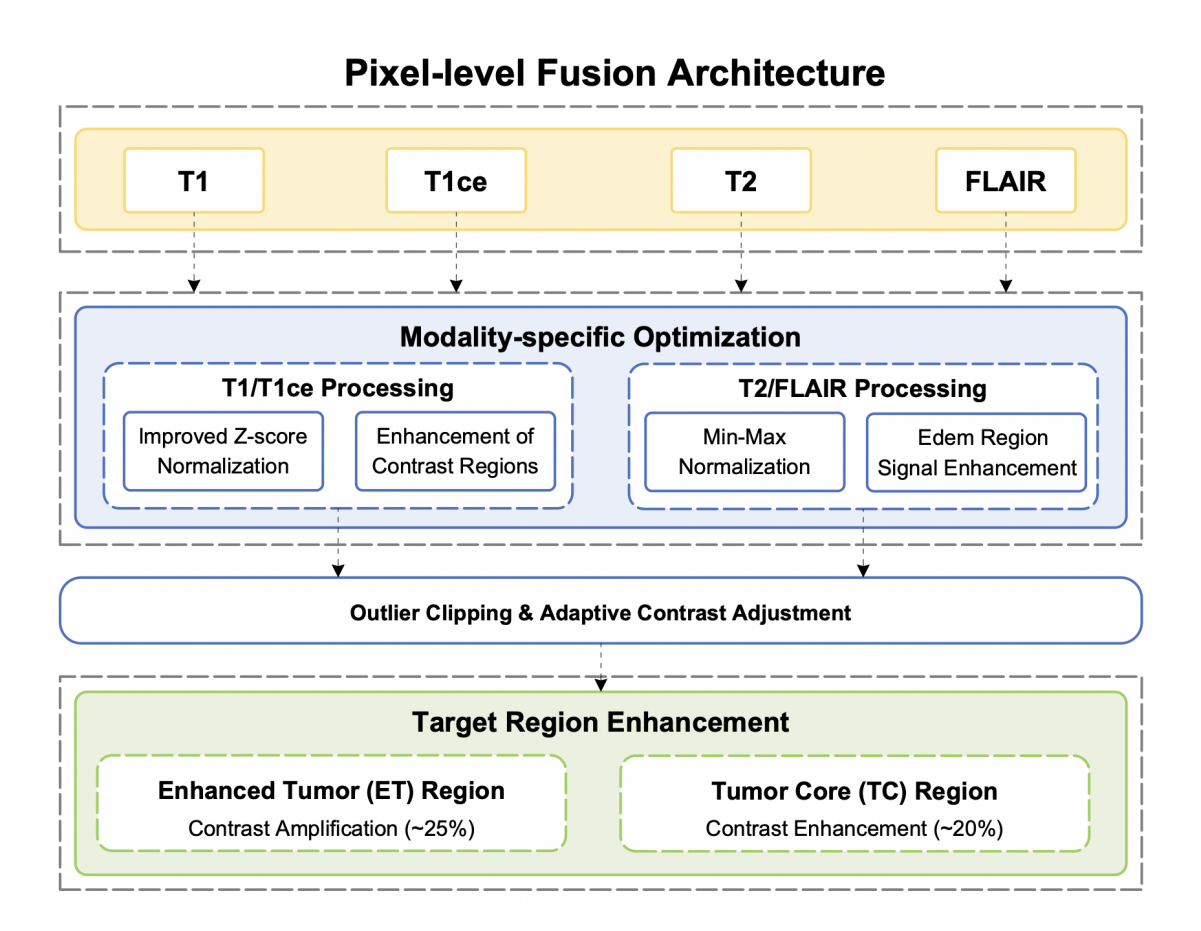


Figure 2: Pixel-level fusion architecture diagram

3.3 Feature-Level Fusion

Feature-level fusion implements multi-scale and multi-modal information integration through an enhanced 3D U-Net segmentation network with four components: attention-enhanced residual blocks, multi-level feature extraction, deep supervision mechanisms, and region-specific feature enhancement [2].

Attention-enhanced residual blocks integrate residual connections and convolutional block attention modules (CBAM), enabling the network to attend to feature channels and spatial positions. These mechanisms implement multi-scale self-guided attention principles relevant for medical image segmentation [22]. Multi-level feature extraction adopts an encoder-decoder structure with the encoder path containing four blocks, gradually increasing base channel numbers from 32 to 512, while the decoder path upsamples feature maps and merges corresponding encoder layer features through skip connections. We incorporate attention gating mechanisms for ET and TC regions in decoder blocks and implement deep supervision mechanisms through auxiliary segmentation heads at multiple decoder levels. Region-specific feature enhancement generates spatial attention maps to modulate final segmentation predictions.

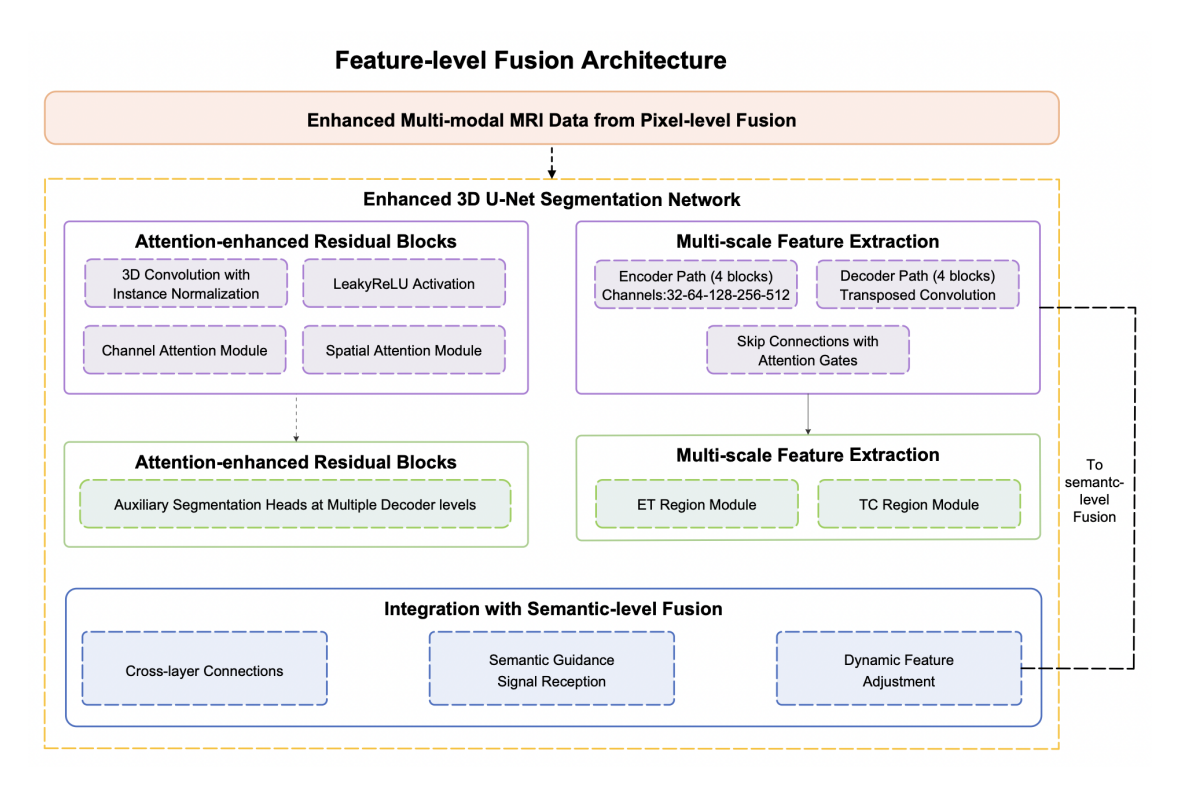


Figure 3: Feature-level fusion architecture diagram

3.4 Semantic-Level Fusion

3.4.1 3D-2D Semantic Bridging

3D-2D semantic bridging addresses the dimensional difference between vision-language models' 2D foundation and 3D medical data [9]. We extract representative slices from three main anatomical planes using projection axis sets:

$$P_{axial} = (0, 1, 2), P_{coronal} = (0, 2, 1), P_{sagittal} = (1, 2, 0)$$
(1)

Where P_{axial} , $P_{coronal}$, and $P_{sagittal}$ represent coordinate axis arrangements of axial, coronal, and sagittal planes respectively, used to rearrange 3D volumetric data for extracting slices from corresponding planes. Each triplet contains numbers representing axis indices in the original volume coordinate system.

For each view direction, we rearrange volume data axes, extract center slices, enhance key features through a 2D processing network, resize to 224×224, and extract features through CLIP's visual model. Features from different views are averaged to form a unified 3D understanding:

$$F_{3D} = \frac{1}{3} \sum_{d \in \{axial, coronal, sagittal\}} F_{cls}^d$$
 (2)

Where F_{3D} represents the final unified 3D volume representation, F_{cls}^d represents the [CLS] token features obtained from slices extracted from direction d (axial, coronal, or sagittal) through the CLIP visual encoder, and the summation operation averages features across the three main anatomical planes to form a 3D representation.

3.4.2 Cross-Modal Semantic Guidance

Cross-modal semantic guidance implements text description guidance for visual feature extraction. We process medical descriptions through CLIP's text encoder and transform visual and text features into shared semantic space through dedicated mappers.

We design a semantic gating fusion mechanism that generates text-based modulation signals applied to visual features:

$$G_{text} = \sigma(F_{text\ mapped}) \tag{3}$$

Where G_{text} represents the gating signal generated from text features, σ represents the sigmoid activation function normalizing outputs to 0-1 range, and F_{text_mapped} represents text features processed through mapping layers.

$$F_{combined} = F_{vision_mapped} \odot G_{text} + F_{text_mapped} \odot (1 - G_{text})$$

$$\tag{4}$$

Where $F_{combined}$ represents the fusion result of visual and text features, F_{vision_mapped} represents visual features processed through mapping layers, \odot represents element-wise multiplication (Hadamard product), and the equation implements adjustment of visual features based on text content.

This gating mechanism allows the model to adjust visual feature weights based on medical description content, guiding the segmentation process toward regions mentioned in descriptions [18]. Fused features are processed through multi-head self-attention mechanisms to generate the final semantically enhanced representation:

$$F_{fused} = \text{LayerNorm}(F_{combined} + \text{MultiHead}(F_{combined})) \tag{5}$$

Where F_{fused} represents the final fused features after attention processing, MultiHead represents multi-head self-attention operations enhancing internal relationship modeling, LayerNorm represents layer normalization stabilizing the training process, and the plus sign represents residual connections ensuring transmission of original feature information. This approach builds upon asymmetric dual network principles examined in medical image fusion contexts [26].

3.4.3 Semantic Attention Enhancement

Semantic attention enhancement transforms semantic understanding into spatial attention allocation. We modulate features through semantic gating units at the network bottleneck layer and design semantically enhanced attention modules for ET and TC regions, generating spatial attention maps to modulate segmentation predictions:

$$Y_{ET_enhanced} = Y_{base_ET} \odot \sigma(f_{conv}(F_{decoder1}, F_{fused}))$$
(6)

Where $Y_{ET_enhanced}$ represents enhanced tumor region segmentation results, Y_{base_ET} represents initial predictions for ET regions from the base segmentation network, $F_{decoder1}$ represents feature maps from the first decoder layer containing spatial details, F_{fused} represents semantic feature representation from fused visual and text modalities, f_{conv} represents an attention network composed of convolutional layers generating spatial attention maps, and σ represents the sigmoid activation function normalizing outputs to 0-1 range.

The final segmentation results consist of three channels corresponding to WT, TC, and ET regions:

$$Y_{final} = [Y_{WT}, Y_{TC_enhanced}, Y_{ET_enhanced}] \tag{7}$$

Where Y_{final} represents the final multi-channel segmentation results, Y_{WT} represents whole tumor region predictions including all abnormal regions, $Y_{TC_enhanced}$ represents tumor core region predictions enhanced through semantic attention, and $Y_{ET_enhanced}$ represents enhancing tumor region predictions enhanced through semantic attention. Square brackets represent concatenation of the three single-channel predictions into multi-channel output.

We also incorporate conditional batch normalization in segmentation heads and support tumor type classification as part of a multi-task learning framework.

4 Results

4.1 Dataset and Experimental Setup

This study utilized the BraTS 2020 dataset, comprising 369 multi-institutional MRI scans with four co-registered sequences (T1, T1ce, T2, FLAIR) at isotropic 1mm³ resolution and expert-annotated ground truth for three clinically significant tumor regions (WT, TC, ET) [15]. Methodological consistency was maintained through 5-fold cross-validation conducted on NVIDIA A100 GPU infrastructure, with the medical CLIP adapter initialized using pre-trained CLIP ViT-B/32 weights and the 3D U-Net backbone employing Kaiming initialization. Optimization protocol utilized the Adam algorithm (initial learning rate: 1e-4) with cosine annealing, weight decay (1e-5), and dropout regularization (0.2), supplemented by data augmentation strategies including random flipping, rotation, and intensity modulation to enhance model generalizability. Performance assessment employed dual complementary metrics: the Dice coefficient (range: 0-1) quantifying volumetric overlap between predicted and ground truth segmentations, and the 95% Hausdorff distance (HD95, measured in millimeters) evaluating boundary localization precision by calculating the maximum surface distance between segmentation boundaries after outlier exclusion, with higher Dice values and lower HD95 measurements indicating improved segmentation accuracy [3].

4.2 Model Training Dynamics and Visual Results Analysis

4.2.1 Training Convergence Characteristics

To analyze the temporal evolution of model performance during training, we tracked the validation metrics across training epochs for all tumor subregions. Figure 4 illustrates the progression of HD95 (boundary localization precision) and Dice coefficient (volumetric overlap) on the validation set, providing insights into the learning dynamics of the architecture.

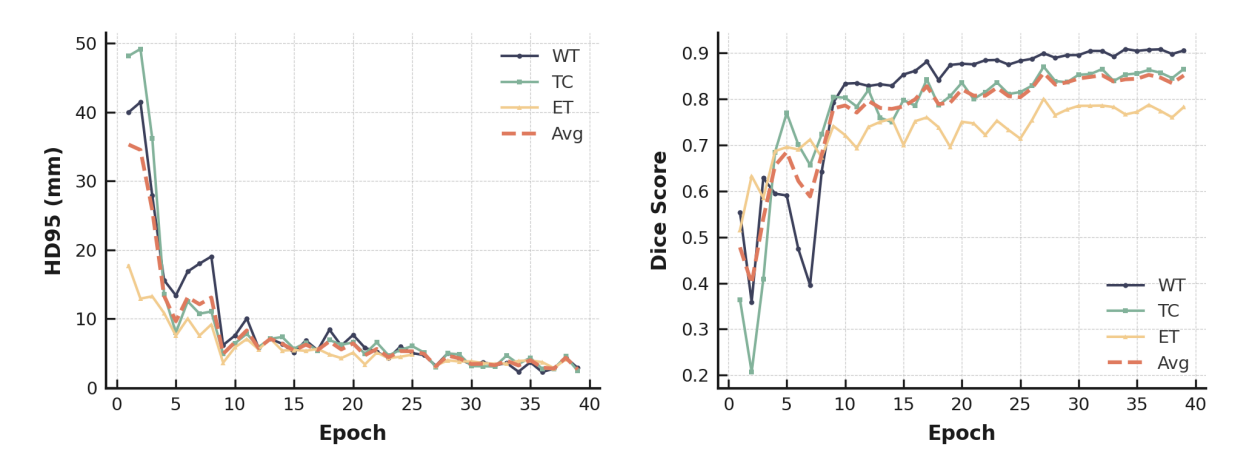


Figure 4: Three-layer fusion architecture training dynamics analysis: (left) HD95 boundary localization precision temporal evolution; (right) volume overlap accuracy (Dice) convergence curves

The HD95 metric exhibits initial variability (TC regions \approx 50mm) followed by an inflection point at epochs 8-10 coinciding with semantic fusion activation, ultimately achieving values below 5mm across all regions by epoch 30. Dice coefficients demonstrate more consistent progression, reaching 0.90 (WT), 0.87 (TC), and 0.80 (ET) by training conclusion. This convergence pattern indicates heterogeneous tumor regions require extended epochs (25-30) for full activation of multi-level mechanisms, reflecting the integration of semantic fusion components with lower-level processes.

4.2.2 Segmentation Result Quality Assessment

To evaluate the qualitative performance of the segmentation framework, we conducted visual assessment of representative cases with varying difficulty levels. Figure 5 presents a comparison of segmentation results between the proposed framework (Base) and traditional 3D U-Net, using color-coded overlays that represent whole tumor (red), tumor core (green), and enhancing tumor (blue) regions.

The Base model exhibits different characteristics in tumor contour delineation and structural representation compared to traditional 3D U-Net, particularly in challenging cases where conventional approaches show segmentation variations. This performance difference relates to the hierarchical processing strategy—pixel-level optimization, feature-level enhancement, and semantic-level guidance—which reflects elements of radiologists' diagnostic approach in integrating perceptual features with conceptual understanding [24].

4.3 Quantitative Results Analysis

To systematically evaluate the contribution of individual fusion components, we conducted ablation experiments by selectively removing each architectural layer. Table 1 presents the performance comparison across different model configurations using the dual-metric evaluation system of Dice coefficient and 95% Hausdorff distance (HD95). The complete Base model serves as the reference standard, while traditional 3D-UNet provides a technical baseline for comparative analysis.

The Base model shows improvements over traditional 3D-UNet (Dice: +4.79%, HD95: -36.2%), with enhanced tumor regions demonstrating larger differences (Dice: +7.28%, HD95: -44.9%). Component ablation reveals dependencies: feature fusion removal leads to model failure, while pixel and semantic fusion removal produce moderate Dice

^{*} Absence of feature-level fusion layer results in model output limited to background classification.

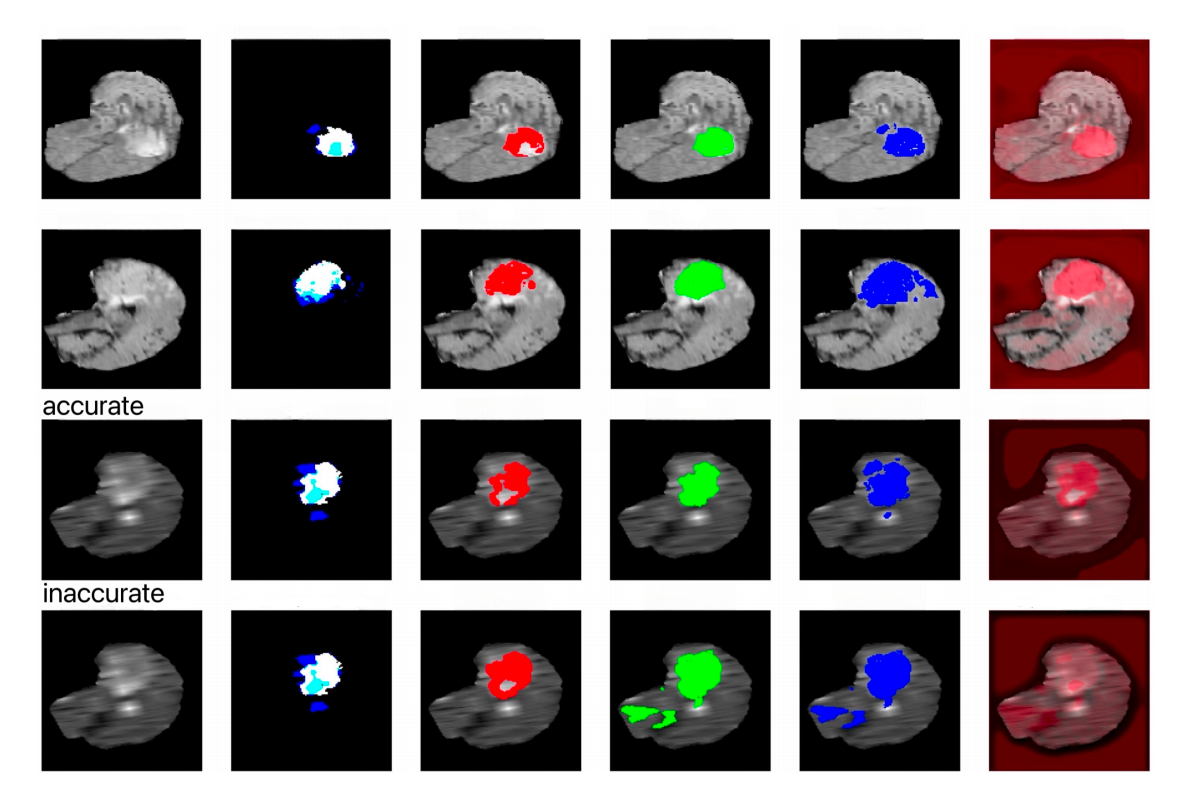


Figure 5: Brain tumor segmentation result visualization. Color overlay demonstrates segmentation effects, with red for WT regions, green for TC regions, and blue for ET regions. The top row shows high-precision cases, bottom row shows challenging cases, with the Base model demonstrating different tumor contour delineation compared to traditional 3D U-Net.

Table 1: Fusion Layer Ablation Experimental Results

Model	Avg_Dice	Avg_HD95	WT_Dice	TC_Dice	ET_Dice	WT_HD95	TC_HD95	ET_HD95
Base	0.8567	3.0972	0.8994	0.8702	0.8005	3.1612	2.9667	3.1638
-Pixel Fusion Layer	0.8435	3.4298	0.8812	0.8534	0.796	3.816	3.2754	3.1979
-Feature Fusion Layer*	0.0	-	0.0	0.0	0.0	-	-	-
-Semantic Fusion Layer	0.8433	3.6729	0.8959	0.8525	0.7815	3.445	3.7158	3.858
Traditional 3D-UNet	0.8088	4.8528	0.8887	0.8099	0.7277	3.7392	5.0812	5.7379

reductions (1.32% and 1.34% respectively) but different HD95 changes (10.7% and 18.6%). This indicates feature-level mechanisms provide foundational representations, while semantic-level components contribute differently to boundary precision in heterogeneous regions—findings with relevance for treatment planning applications [11].

4.4 Feature Extraction Strategy Evaluation

To assess the impact of different feature extraction approaches on segmentation performance, we conducted comparative experiments across multiple architectural variants while maintaining the overall three-layer fusion framework. Table 2 presents performance metrics for the Base model, 3D ResNet, 2D ResNet50, and a configuration with no feature extractor. This experiment evaluates the dimensional adaptability and feature quality contributions to the segmentation task.

Feature extraction analysis reveals dimensional effects, with the Base model differing from 3D ResNet (Dice: +1.03%, HD95: -8.7%) and 2D ResNet50 (Dice: +18.66%, HD95: -66.7%). 2D approaches show reduced performance in volumetric regions (WT Dice: 0.5336, HD95: 14.2685mm), indicating three-dimensional extraction's utility for spatial continuity preservation. Between 3D variants, performance differences in whole tumor boundary localization (40.0%)

^{*} Absence of feature extractors prevents effective feature representation establishment.

Table 2: Feature Extraction Strategy Evaluation Results

Model	AVG_Dice	AVG_HD95	WT_Dice	TC_Dice	ET_Dice	WT_HD95	TC_HD95	ET_HD95
Base	0.8567	3.0972	0.8994	0.8702	0.8005	3.1612	2.9667	3.1638
3D ResNet	0.8464	3.394	0.8923	0.8563	0.7905	5.2736	2.4531	2.4553
2D ResNet50	0.6701	9.3031	0.5336	0.7745	0.7023	14.2685	7.026	6.615
No Feature Extractor*	0.0	-	0.0	0.0	0.0	-	-	-

HD95 difference for Base model) suggest attention mechanisms affect contextual representation. These findings inform architectural considerations in clinical deployment contexts, particularly for resource-constrained environments.

4.4.1 Semantic Fusion Mechanism Ablation Analysis

To examine the functional distribution of components within the semantic fusion layer, we conducted targeted ablation experiments on specific mechanisms. Table 3 presents performance comparisons between the complete Base model, traditional 3D-2D fusion methods, variants without semantic guidance, and variants without semantic attention. This component-level analysis provides insights into the relative contributions of individual semantic processing modules.

Table 3: Semantic Fusion Mechanism Ablation Analysis Results

Model	AVG_Dice	AVG_HD95	WT_Dice	TC_Dice	ET_Dice	WT_HD95	TC_HD95	ET_HD95
Base	0.8567	3.0972	0.8994	0.8702	0.8005	3.1612	2.9667	3.1638
Traditional 3D-2D	0.8476	2.8836	0.9066	0.8593	0.777	2.2724	2.9277	3.4507
-Semantic Guidance	0.8532	4.0712	0.9064	0.8598	0.7935	3.383	4.1066	4.7239
-Semantic Attention	0.8491	2.9268	0.909	0.8562	0.7821	2.3942	2.7221	3.6642

Semantic component analysis reveals functional patterns: guidance mechanisms show limited impact on volumetric overlap (Dice: -0.35% when removed) but affect boundary precision (HD95: +31.4%, ET regions: +49.3%), indicating their relationship to delineation through contextual understanding. Attention mechanisms demonstrate region-specific effects, with removal affecting ET Dice (-1.84%) but showing different patterns in WT metrics (Dice: +0.96%, HD95: -24.3%), suggesting resource allocation across tumor subregions. This distribution enables application-specific adjustment based on clinical priorities.

4.4.2 Tumor Region-Specific Analysis

To assess the adaptability of the proposed architecture to different pathological tissue types, we conducted region-specific performance analysis across tumor subcomponents. Table 4 evaluates segmentation accuracy for non-enhancing tumor/necrosis (NCR/NET), peritumoral edema (ED), and enhancing tumor (ET) regions across different model configurations. This analysis provides clinical perspective on the architecture's utility for specific diagnostic and treatment planning applications.

Table 4: Tumor Region-Specific Analysis Results

Model	NCR/NET_Dice	ED_Dice	ET_Dice
Base	0.785	0.807	0.8372
Traditional 3D-2D	0.7819	0.802	0.8164
-Semantic Guidance	0.7768	0.805	0.8297
-Semantic Attention	0.7746	0.8007	0.8236

Region-specific analysis demonstrates tissue-dependent component contributions, with the Base model showing different performance in enhancing tumor regions (Dice: 0.8372, +2.08% versus traditional methods) while conventional approaches maintain differences in NCR/NET regions (+0.31%). Component contributions exhibit patterns—semantic guidance affects NCR/NET segmentation while attention mechanisms influence ET region delineation. This specificity relates to imaging characteristics: enhancing regions show interaction with attention-based feature modification, while necrotic regions demonstrate relationships with semantic guidance [26].

5 Discussion

The proposed three-layer fusion architecture addresses certain limitations in brain tumor segmentation through integration of information across multiple domains. This hierarchical framework establishes a processing sequence from pixel-level optimization of modality-specific characteristics to feature-level spatial representation via attention-enhanced mechanisms, incorporating semantic-level integration of professional knowledge. The multi-level integration approach aligns with approaches in medical image analysis that recognize the complementary nature of different processing scales, particularly for heterogeneous tumor regions where conventional approaches face challenges [23, 24]. Performance metrics demonstrate changes in both volumetric overlap accuracy and boundary delineation precision, with measurable differences observed across tumor subregions of varying complexity.

The semantic-level fusion pathway presents a methodological approach through three mechanisms: 3D-2D semantic bridging addresses dimensional differences between CLIP's two-dimensional foundation [5] and volumetric medical data; cross-modal semantic guidance transfers information from radiological descriptions to visual feature processing via text-based gating; and semantic attention enhancement transforms conceptual understanding into spatial feature modulation. This approach addresses a limitation of current methods that typically underutilize semantic knowledge embedded in medical reports, as examined in vision-language modeling for medical applications [9]. Ablation analyses indicate that semantic components contribute to enhancing tumor (ET) delineation, with a 7.3% Dice coefficient difference in these clinically significant regions.

The clinical implications of these findings are noteworthy, as segmentation accuracy affects treatment planning precision, particularly for radiation therapy where boundary definition influences both therapeutic outcomes and adverse effect profiles [1]. The differential performance patterns across tumor subregions indicate potential for application-specific adjustment, allowing clinical teams to prioritize segmentation accuracy for specific pathological components based on treatment requirements [15]. This targeted approach to segmentation represents a development in the application of deep learning methodologies for neuro-oncological intervention planning.

6 Conclusion

This research presents a multi-level fusion architecture that integrates vision-language models with three-dimensional medical volumetric data through a hierarchical processing chain. The proposed framework addresses challenges in cross-dimensional representation and domain adaptation through three components: pixel-level preprocessing optimization, feature-level spatial representation, and semantic-level cross-modal guidance. Experimental validation demonstrates performance differences, with the model achieving an overall Dice coefficient of 0.8567 (4.79% difference compared to traditional 3D U-Net), with changes in enhancing tumor regions (7.28% Dice difference, 44.9% HD95 difference). Ablation studies indicate the contributions of each fusion layer, while region-specific analysis reveals segmentation patterns across heterogeneous tumor tissue types.

Future research will examine the extension of this approach to additional three-dimensional medical segmentation tasks, developing semantic guidance mechanisms, and exploring interpretable attention frameworks to enhance clinical decision support [27].

Acknowledgments

Not applicable.

Declarations

- Funding: Not applicable.
- Conflict of interest/Competing interests: The author declares no competing interests.
- Ethics approval and consent to participate: Not applicable.
- Consent for publication: Not applicable.
- Availability of data and materials: The BraTS 2020 dataset analyzed in this study is publicly available at the Brain Tumor Segmentation (BraTS) challenge website: https://www.med.upenn.edu/cbica/brats2020/.
- Materials availability: Not applicable.
- Code availability: The implementation code is available from the corresponding author on reasonable request.

• Authors' contributions: The author was responsible for all aspects of the study.

Appendix A. Implementation Details

The implementation was conducted in Python 3.8.5 using PyTorch 1.12.1 on Ubuntu 20.04 with an NVIDIA Tesla V100 GPU (32 GB). Primary dependencies included NumPy 1.21.5, SciPy 1.7.3, SimpleITK 2.1.1, Transformers 4.15.0, and nibabel 3.2.1.

A.1 Hyperparameter Configuration

All experiments used a batch size of 1 and the AdamW optimizer with weight decay 1×10^{-4} . Learning rates were scheduled by OneCycleLR with cosine annealing (pct_start = 0.2, div_factor = 20, final_div_factor = 100), initial rate 5×10^{-5} , and parameter-group multipliers:

- Encoder & Decoder parameters: 2× base rate
- CLIP adapter parameters: $0.1 \times$ base rate
- Attention module parameters: 3× base rate

Dropout was set to 0.1 in CLIP adapter layers and 0.3/0.2 in the tumor classification head. Mixed-precision training was enabled via torch.cuda.amp.GradScaler.

A.2 Data Augmentation

On-the-fly augmentation included:

- Random flips per spatial dimension, p = 0.5
- Random rotations in $[-15^{\circ}, +15^{\circ}], p = 0.3$
- Intensity scaling via gamma correction $\gamma \sim \mathcal{U}(0.8, 1.2), p = 0.3$
- Tumor-focused cropping when masks exist
- Contrast stretching factors of 1.25 (ET) and 1.2 (TC), p = 0.5

A.3 Preprocessing

Intensity normalization per modality:

- T1, T1ce: z-score over the brain mask
- T2, FLAIR: min-max scaling, clipped to [-5, +5]
- T1ce contrast boost: exponentiation by 0.9 after clipping

The full codebase is available from the corresponding author upon reasonable request.

References

- [1] Ali, A., Syed, S. M., Syed, A. H., et al.: Brain tumor segmentation with deep learning: BraTS challenges from 2012 to 2020. IEEE Trans Med Imaging **40**(10), 2557–2567 (2022). https://doi.org/10.1109/TMI.2021.3070449
- [2] Myronenko, A.: 3D MRI brain tumor segmentation using autoencoder regularization. In: Brainlesion: Glioma, Multiple Sclerosis, Stroke and Traumatic Brain Injuries, pp. 311–320. Springer (2019). https://doi.org/10.1007/978-3-030-11726-9_28
- [3] Yogananda, C. G. B., Shah, B. R., Vejdani-Jahromi, M., et al.: A fully automated deep learning network for brain tumor segmentation. Tomography 6(2), 186–193 (2020). https://doi.org/10.18383/j.tom.2020.00024
- [4] Chen, L., Cui, H., Zhang, K.: ANU-Net: Attention-based nested U-Net to exploit full resolution features for medical image segmentation. Comput Graph 90, 11–20 (2020). https://doi.org/10.1016/j.cag.2020.05. 003

- [5] Radford, A., Kim, J. W., Hallacy, C., et al.: Learning transferable visual models from natural language supervision. In: Proceedings of the 38th International Conference on Machine Learning, pp. 8748–8763. PMLR (2021)
- [6] Vaswani, A., Shazeer, N., Parmar, N., et al.: Attention is all you need. In: Advances in Neural Information Processing Systems, vol. 30 (2017)
- [7] Zhang, S., Xu, Y., Usuyama, N., et al.: Large-scale domain-specific pretraining for biomedical vision-language processing. arXiv preprint arXiv:2303.00915 (2023)
- [8] Qiu, Z., Li, J., Wang, X., et al.: 3D Multimodal Fusion Network with Disease-induced Joint Learning for Early Alzheimer's Disease Diagnosis. IEEE Trans Med Imaging (in press) (2024). https://doi.org/10.1109/TMI. 2024.3352731
- [9] Liu, J., Zhang, Y., Chen, J., et al.: Universal and Extensible Language-Vision Models for Organ Segmentation and Tumor Detection from Abdominal Computed Tomography. Med Image Anal **87**, 102847 (2024). https://doi.org/10.1016/j.media.2023.102847
- [10] Menze, B. H., Jakab, A., Bauer, S., et al.: The multimodal brain tumor image segmentation benchmark (BRATS). IEEE Trans Med Imaging **34**(10), 1993–2024 (2014). https://doi.org/10.1109/TMI.2014.2377694
- [11] Zeineldin, R. A., Karar, M. E., Burgert, O., et al.: Multimodal CNN Networks for Brain Tumor Segmentation in MRI: A BraTS 2022 Challenge Solution. In: Brainlesion: Glioma, Multiple Sclerosis, Stroke and Traumatic Brain Injuries, pp. 124–136 (2023). https://doi.org/10.1007/978-3-031-44366-4_10
- [12] Yuan, Y.: Automatic brain tumor segmentation with scale attention network. In: Brainlesion: Glioma, Multiple Sclerosis, Stroke and Traumatic Brain Injuries, pp. 285–294. Springer (2021). https://doi.org/10.1007/978-3-030-72087-2_25
- [13] Wang, W., Chen, C., Ding, M., et al.: TransBTS: Multimodal brain tumor segmentation using transformer. In: Medical Image Computing and Computer Assisted Intervention, pp. 109–119. Springer (2021). https://doi.org/10.1007/978-3-030-87193-2_11
- [14] Zhou, C., Ding, C., Wang, X., et al.: One-pass multi-task networks with cross-task guided attention for brain tumor segmentation. IEEE Trans Image Process 29, 4516–4529 (2020). https://doi.org/10.1109/TIP. 2020.2973510
- [15] Bakas, S., Reyes, M., Jakab, A., et al.: Identifying the Best Machine Learning Algorithms for Brain Tumor Segmentation, Progression Assessment, and Overall Survival Prediction in the BRATS Challenge. arXiv preprint arXiv:1811.02629 (2018)
- [16] Li, X., Jiang, Y., Li, M., et al.: MSFR-Net: Multi-modality and single-modality feature recalibration network for brain tumor segmentation. Med Phys **50**(4), 2249–2262 (2023). https://doi.org/10.1002/mp.16049
- [17] Liu, J., Zhang, Y., Wang, K., et al.: CLIP-Driven Universal Model for Organ Segmentation and Tumor Detection. In: Proceedings of the IEEE/CVF International Conference on Computer Vision, pp. 12039–12049 (2023). https://doi.org/10.1109/ICCV.2023.01160
- [18] Adhikari, R., Dhakal, M., Bhandari, P., et al.: Vision Language Model for Interpretable Medical Image Segmentation. In: Medical Imaging with Deep Learning (2023)
- [19] Poudel, K., Dhakal, M., Bhandari, P., et al.: Exploring Transfer Learning in Medical Image Segmentation using Vision-Language Models. In: MIDL 2024 (2024)
- [20] Guo, M., Yi, H., Qin, Z., et al.: Multiple prompt fusion for zero-shot lesion detection using vision-language models. In: Medical Image Computing and Computer Assisted Intervention, pp. 283–292. Springer (2023). https://doi.org/10.1007/978-3-031-43996-4_27
- [21] Algarni, A. D.: Automated medical diagnosis system based on multi-modality image fusion and deep learning. Sci Rep 13(1), 7528 (2023). https://doi.org/10.1038/s41598-023-34657-z
- [22] Sinha, A., Dolz, J.: Multi-scale self-guided attention for medical image segmentation. IEEE J Biomed Health Inform 25, 121–130 (2021). https://doi.org/10.1109/JBHI.2020.2986926
- [23] Wen, J., Liu, L., Ye, B., et al.: Msgfusion: medical semantic guided two-branch network for multimodal brain image fusion. IEEE Trans Multimedia 26, 944–957 (2023). https://doi.org/10.1109/TMM.2023.3245476
- [24] Zhu, Z., Liang, H., Han, Y., et al.: Brain tumor segmentation based on the fusion of deep semantics and edge information in multimodal MRI. Inf Fusion 91, 376–387 (2023). https://doi.org/10.1016/j.inffus.2022.12.004
- [25] Huang, Z., Lin, L., Cheng, P., et al.: Multi-modal brain tumor segmentation via missing modality synthesis and modality-level attention fusion. arXiv preprint arXiv:2203.04586 (2022)

- [26] Huang, W., Ma, S., Liu, F., et al.: ADDNS: An asymmetric dual deep network with sharing mechanism for medical image fusion of CT and MR-T2. Comput Biol Med 166, 107531 (2023). https://doi.org/10.1016/j.compbiomed.2023.107531
- [27] Karri, M., Annavarapu, C. S. R., Acharya, U. R.: Explainable multi-module semantic guided attention based network for medical image segmentation. Comput Biol Med **151**, 106231 (2022). https://doi.org/10.1016/j.compbiomed.2022.106231